Article
pubs.acs.org/Biomac

Complexes of Magnetic Nanoparticles with Cellulose Nanocrystals as Regenerable, Highly Efficient, and Selective Platform for Protein Separation

Jiaqi Guo,[†] Ilari Filpponen,[*,†,‡] Leena-Sisko Johansson,[†] Pezhman Mohammadi,[‡] Mika Latikka,[∥] Markus B. Linder,[‡] Robin H. A. Ras,[∥] and Orlando J. Rojas[†,⊥,∥]

[†]Department of Bioproducts and Biosystems, School of Chemical Engineering, Aalto University, FI-00076 Aalto, Finland

[‡]Alabama Center for Paper and Bioresource Engineering, Department of Chemical Engineering, Auburn University, Auburn, Alabama 36849-5127, United States

[∥]Department of Applied Physics, School of Science, Aalto University, FI-00076 Aalto, Finland

[⊥]Departments of Forest Biomaterials and Chemical and Biomolecular Engineering, North Carolina State University, Raleigh, North Carolina 27695, United States

Supporting Information

ABSTRACT: We present an efficient approach to develop cellulose nanocrystal (CNC) hybrids with magnetically responsive Fe_3O_4 nanoparticles that were synthesized using the (Fe^{3+}/Fe^{2+}) coprecipitation. After 2,2,6,6-tetramethylpiperidine-1-oxyl radical (TEMPO)-catalyzed oxidation of CNC, carbodiimide (EDC/NHS) was used for coupling amine-containing iron oxide nanoparticles that were achieved by dopamine ligand exchange (NH_2−Fe_3O_4 NPs). The as-prepared hybrids (Fe_3O_4@CNC) were further complexed with Cu(II) ions to produce specific protein binding sites. The performance of magnetically responsive Cu−Fe_3O_4@CNC hybrids was assessed by selectively separating lysozyme from aqueous media. The hybrid system displayed a remarkable binding capacity with lysozyme of 860.6 ± 14.6 mg/g while near full protein recovery (~98%) was achieved by simple elution. Moreover, the regeneration of Fe_3O_4@CNC hybrids and efficient reutilization for protein separation was demonstrated. Finally, lysozyme separation from matrices containing egg white was achieved, thus revealing the specificity and potential of the presented method.

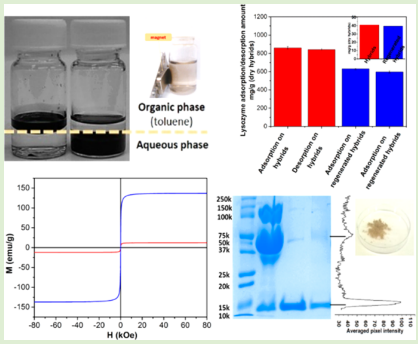

INTRODUCTION

Proteins play an important role in materials science and biotechnological/biopharmaceutical industries.[1,2] Therefore, considerable efforts have been devoted to obtain highly purified proteins which may have properties such as antimicrobiality (antivirality), photoactivity, elasticity, and redox potential.[3−7] Conventional methods to separate proteins include chromatography, precipitation, crystallization, centrifugation, and membrane-based techniques. However, a low adsorption capacity (related to the available surface area) and an insufficient separation efficiency are some of the major drawbacks of these methods. Therefore, substrates possessing large specific surface area (SSA) such as cellulose nanocrystals (CNC) are promising candidates for enhanced protein separation/purification; in particular, the combination of large SSA and magnetic responsiveness can be of great impact in the field.

CNC can be isolated from various botanical sources such as wood, straw, and cotton by using top-down methods.[8] Rod-shaped CNC particles possess high aspect ratio (typically 20−50), high surface area (419 m^2/g), and high mechanical strength.[9,10] These features, as well as their abundance, low density, the suitability for surface functionalization, ability to self-assemble, and so forth, make CNC useful in developing new biobased nanomaterials, such as those comprising polymer nanocomposites, mechanically adaptive systems, hydro/aerogels, and thin films, among others.[11−16] Moreover, magnetically responsive nanocellulose materials have been investigated in medical applications,[17] transparent films,[18] electrospun polyvinyl alcohol (PVA)-CNC composite fibers,[19] and aerogels.[20]

Magnetic nanoparticles such as MFe_2O_4 (M = Co, Fe, Ni), CoFe, FePt, and $SmCo_5$ can be synthesized via coprecipitation, thermal decomposition and/or reduction, and hydrothermal synthesis.[21] They have been used in catalytic, biomedical, drug delivery, and magnetic resonance imaging (MRI) applications.[22−26] Moreover, the separation of biomolecules using magnetic nanoparticles has been demonstrated.[27,28] For example, Xu et al. employed nickel-nitrilotriacetic acid complex-conjugated magnetic nanoparticles that showed

Received: November 30, 2016
Revised: February 10, 2017
Published: February 15, 2017

DOI: 10.1021/acs.biomac.6b01778
Biomacromolecules 2017, 18, 898−905

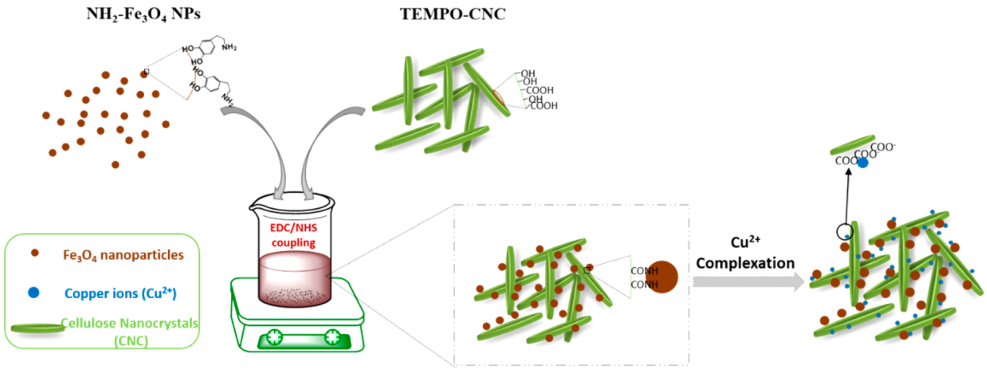

Figure 1. Schematic illustration of the preparation of copper-complexed Fe_3O_4@CNC hybrids. Amino-functionalized Fe_3O_4 NPs were synthesized using the (Fe^{3+}/Fe^{2+}) coprecipitation method and followed by dopamine ligand exchange. TEMPO-CNC were prepared via TEMPO-mediated oxidation. Magnetically responsive Fe_3O_4@CNC hybrids are prepared by EDC/NHS-assisted coupling of TEMPO-CNC and $NH_2-Fe_3O_4$ NPs. Copper ions were complexed onto Fe_3O_4@CNC hybrids to provide specific binding sites for the protein, for example, lysozyme.

excellent separation performance for histidine-tagged proteins.[29] Moreover, an investigation from Lee et al. indicated that the imidazole-stabilized Ni/NiO core/shell nanoparticles could be used for the separation of histidine-tagged proteins.[30] Attempts to utilize cellulose-containing magnetic substrates for protein separation and enzyme immobilization have also been reported.[31−33] However, the selective separation of proteins from a complex natural substrate by using cellulose-based magnetic nanoparticles has remained a challenge.

In this work, an efficient and scalable approach for selective protein separation from a complex mixture via magnetically responsive Fe_3O_4@CNC hybrids is presented. First, the primary hydroxyl groups on the surface of the CNC were selectively oxidized to corresponding carboxyl groups via 2,2,6,6-tetramethyl-1-piperidinyloxyradical (TEMPO)-mediated oxidation. Concurrently, amino-functionalized Fe_3O_4 nanoparticles (NPs) were synthesized using the (Fe^{3+}/Fe^{2+}) coprecipitation method. Next, *N*-(3-(dimethylamino)propyl)-*N*′-ethylcarbodiimide hydrochloride/*N*-hydroxysuccinimide (EDC/NHS)-assisted coupling of TEMPO-oxidized cellulose nanocrystals (TEMPO-CNC) and $NH_2-Fe_3O_4$ NPs was employed to produce the magnetically responsive Fe_3O_4@CNC hybrids. The properties of TEMPO-CNC, $NH_2-Fe_3O_4$ NPs, and Fe_3O_4@CNC hybrids were characterized by atomic force microscopy (AFM), transmission electron microscopy (TEM), Fourier transform infrared spectroscopy (FT-IR) and X-ray photoelectron spectroscopy (XPS), respectively. Furthermore, Fe_3O_4@CNC hybrids were complexed with copper ions to provide specific binding sites for proteins (Figure 1). The performance of magnetically responsive Fe_3O_4@CNC hybrids was assessed by separating lysozyme from a standard solution. Finally, the same methodology was employed for the separation of lysozyme from the egg white. The results indicate that the copper-complexed Fe_3O_4@CNC hybrids can be efficiently used for the protein separation.

EXPERIMENTAL SECTION

Chemicals. All chemicals and materials used in this work were of analytical grade without further purification. 4-(2-Hydroxyethyl)-1-piperazineethanesulfonic acid (HEPES), EDC, NHS, TEMPO, sodium hypochlorite (13% NaClO), iron(III) chloride hexahydrate ($FeCl_3\cdot 6H_2O$), iron(II) chloride tetrahydrate ($FeCl_2\cdot 4H_2O$), sodium bromide, lysozyme, oleic acid (OA), and dopamine (DA) were purchased from Sigma-Aldrich, Finland. Hardened ashless filter paper was acquired from Whatman GmbH, Germany. Spectra/por dialysis membrane (MWCO 6000−8000) was purchased from Spectrum Laboratories Inc., U.S.A. Milli-Q (MQ) water (18.2 MΩ·cm) was used for all aqueous solutions preparation.

Preparation of Cellulose Nanocrystals (CNC) and Subsequent TEMPO-Mediated Oxidation (TEMPO-CNC). CNC used in this study were prepared via hydrocholoric acid hydrolysis of ashless filter paper (Whatman Hardened, grade 541) for 3 h and 45 min according to the method detailed by Araki et al.[34] In order to introduce carboxyl groups on CNC surface, TEMPO-mediated oxidation was carried out according to a previously reported method.[35,36] After one-week dialysis against distilled water, the dry content of TEMPO-CNC suspension was determined to be about 5 g/L. The transparent suspension was stored at 4 °C until further use.

Synthesis of Amino Functionalized Superparamagnetic Iron Oxide Nanoparticles ($NH_2-Fe_3O_4$ NPs). The superparamagnetic amino-functionalized iron oxide nanoparticles ($NH_2-Fe_3O_4$ NPs) were synthesized through the coprecipitation method following the procedure outlined by Yao et al.[37] Briefly, 1.5 g of $FeCl_2\cdot 4H_2O$ and 4.1 g of $FeCl_3\cdot 6H_2O$ were dissolved into 100 mL of Milli-Q water in a three-necked flask under N_2 atmosphere. Then, 25 mL of 25% $NH_3\cdot H_2O$ was quickly added under vigorous stir after 15 min stabilization. The solution color changed from orange to black, which indicate for the formation of Fe_3O_4 NPs. Next, the dispersion was heated to 80 °C and 1 mL of oleic acid was slowly added within 1 h. After that, the as-synthesized Fe_3O_4 NPs were extracted from water with 30 mL of toluene. The oleic acid coated Fe_3O_4 NPs ($OA-Fe_3O_4$ NPs) were stored at 4 °C for further use. The dry content of $OA-Fe_3O_4$ NPs in a suspension was determined to be about 6% w/w (in toluene). (Caution: all glassware involved in the synthesis should be washed with aqua regia prior to the experiments). In order to obtain amino-functionalized Fe_3O_4 NPs, 0.2 g of dopamine (dissolved in 1 mL of methanol) was added into 10 mL of $OA-Fe_3O_4$ NPs and the resulting mixture was sonicated for 2 h in an ice bath. Then, the mixture was extensively washed with methanol and water. The dry content of $NH_2-Fe_3O_4$ NPs in aqueous suspension was measured to be about 7.7 g/L. $NH_2-Fe_3O_4$ NPs were stored at 4 °C for further use.

Fabrication of Magnetically Responsive Nanocellulose-Based Hybrids (Fe_3O_4@CNC Hybrids). The magnetically responsive Fe_3O_4@CNC hybrids were prepared via well-established EDC/NHS-assisted coupling reaction. Briefly, EDC (0.30 g) and NHS (0.23 g) were added to a suspension (30 mL in MES buffer, pH 4.5) of TEMPO-oxidized CNCs (5.1 g/L) under vigorous stirring for 15 min. Next, $NH_2-Fe_3O_4$ NPs (3 mL of 7.7 g/L suspension) was added. The reaction was carried out overnight at room temperature. The resulting Fe_3O_4@CNC hybrids were separated magnetically and washed with deionized water. The dry content of Fe_3O_4-CNC hybrids was measured to be about 3.2 g/L.

Complexation of Copper Ions with Fe_3O_4@CNC Hybrids. Complexation of copper ions with the Fe_3O_4@CNC hybrids was

DOI: 10.1021/acs.biomac.6b01778
Biomacromolecules 2017, 18, 898−905

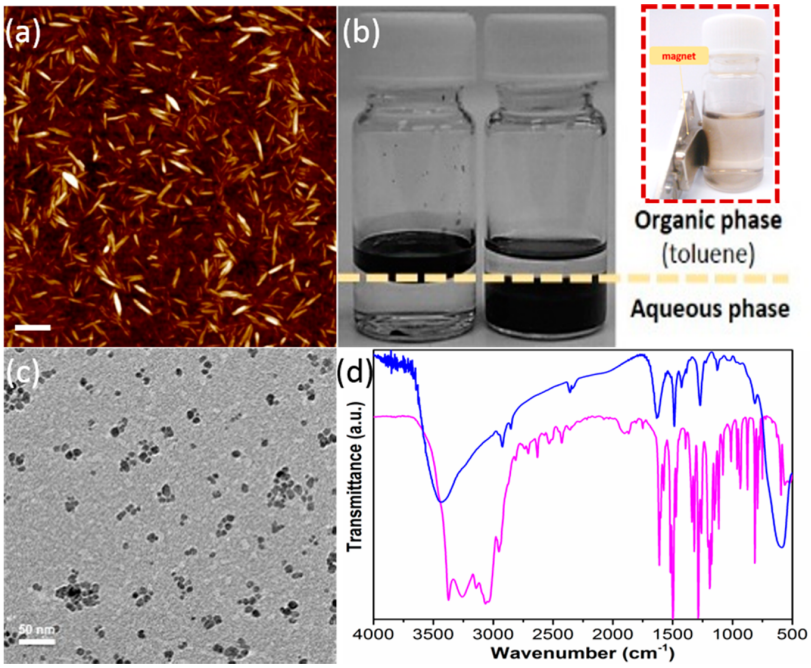

Figure 2. (a) AFM image showing the size of rod-shaped TEMPO-CNC. Scale bar: 300 nm. (b) Photography showing the stability of Fe_3O_4 nanoparticles in toluene (top phase) and water (bottom phase). The left container includes OA− Fe_3O_4 NPs dispersed in toluene and the right one NH_2−Fe_3O_4 NPs dispersed in water. The magnetic responsiveness of NH_2−Fe_3O_4 NPs is shown in the picture on the far right after 3 min. (c) TEM image reveals the size of synthesized Fe_3O_4 NPs (scale bar: 50 nm). (d) FT-IR spectra of NH_2−Fe_3O_4 NPs (upper, blue profile) and pure dopamine compound (bottom, pink curve) revealing the introduction of amino groups onto Fe_3O_4 NPs.

carried out by mixing 4.8 mL of Fe_3O_4@CNC hybrids (3.2 g/L) with 10.2 mL of $CuSO_4$ solution (25 mM, pH = 5) for 2 h at room temperature as described by Zhu et al.[38] Then, the suspension was washed with distilled water under assistance of the external magnetic field until no copper ions could be detected in washing solutions. The Cu^{2+} complexation capacity of Fe_3O_4@CNC hybrids was measured by using Shimadzu UV-2550 spectrophotometer (Shimadzu Corporation, Kyoto, Japan). (See Supporting Information.)

Characterization Methods. FT-IR characterization of TEMPO-CNC, dopamine, NH_2−Fe_3O_4 NPs and Fe_3O_4@CNC hybrids was carried out with a Thermo Scientific Nicolet Avatar 360 FTIR spectrometer in transmittance mode using the KBr pellet technique. Zeta potential of NH_2−Fe_3O_4 NPs (about 1 g/L) was measured with Malvern nano ZS90 (Finland). TEMPO-CNC was characterized in air at room temperature (23 °C) via Multimode AFM with a Nanoscope V controller operated at tapping mode (Bruker Corparation, U.S.A.). Bright-field TEM images of NH_2−Fe_3O_4 NPs and Fe_3O_4@CNC hybrids were acquired using a FEI Tecnai 12 TEM operating at 120 kV. The surface chemical composition of synthesized TEMPO-CNC, NH_2−Fe_3O_4, and magnetically responsive Fe_3O_4@CNC hybrids was investigated using a Kratos Analytical AXIS ultraelectron spectrometer equipped with a monochromatic Al Ka X-ray source at 100 W and a neutralizer. The XPS experiments were performed on the dry thin-films supported by a cleaned silica wafer. In order to obtain consistent results, at least three different areas of each sample were scanned. The thermogravimetric analysis (TGA) of TEMPO-CNC, NH_2−Fe_3O_4, and Fe_3O_4@CNC hybrids was performed via a PerkinElmer TGA7 instrument (Waltham, MA). Prior to heating to 700 °C with a heating rate of 10 °C min^{-1}, approximately 7 mg of sample was dried at 105 °C for 20 min to remove the residual moisture. Nitrogen served as purge gas for TGA measurement. Magnetic properties of the samples (NH_2−Fe_3O_4 and Fe_3O_4@CNC hybrids) were measured using a vibrating sample magnetometer (Quantum Design PPMS Dynacool, Finland). Approximately 5−10 mg of liquid sample was pipetted in standard polypropylene sample holder and sealed with vacuum grease and Parafilm. Hysteresis loops were measured by vibrating the samples with 1 mm peak amplitude and 40 Hz frequency between −9 and +9 T in room temperature.

Protein Binding and Separation from a Predefined Standard Solution. Commercial lysozyme protein was used for assessing the capability of Fe_3O_4@CNC hybrids to bind and separate proteins from a solution. In a typical binding and separation test, 4.8 mL of Fe_3O_4@CNC hybrids was mixed with 6 mL of predefined 1 g/L of lysozyme solution (pH 7) for 2 h at room temperature. Next, Fe_3O_4@CNC hybrids were collected and extensively washed with a buffer solution. The lysozyme binding efficiency was determined by the difference between the initial and final amount of lysozyme in solution, and the concentrations of lysozyme solutions were determined with Shimadzu UV-2550 spectrophotometer (see Supporting Information). The adsorbed protein with the histidine binding unit can be eluted by using high concentrations of salt and imidazole.[39] In order to elute the bound lysozyme, the Fe_3O_4@CNC hybrids were mixed with 8 mL of HEPES (50 mM, pH 8.0) containing 0.3 M imidazole and 0.25 M NaCl for 2 h. Subsequently, the lysozyme concentration in eluent was analyzed. The Fe_3O_4@CNC hybrids were remixed with fresh copper ions as described above for recycling.

Lysozyme Separation from Fresh Egg White. The separation of lysozyme from the fresh chicken egg white was conducted as suggested by Zhu et al.[38] Briefly, egg white collected from the fresh chicken eggs was diluted 3 times with HEPES (50 mM, pH 7.0) and homogenized in an ice bath for 3 h (Polytron PT 2100, Kinematica AG homogenizer). The resulting solution was centrifuged (15 000 rpm) at 4 °C for 30 min, and the supernatant was collected and used as the lysozyme source. Then, 9.6 mL of Fe_3O_4@CNC hybrids were mixed with 20 mL of copper(II) sulfate (25 mM, pH 5.0) for 2 h and washed extensively to remove the excess of copper. The Cu^{2+} complexed Fe_3O_4@CNC hybrids were mixed with 13 mL of egg white solution for 2 h at room temperature. After washing, the elution of lysozyme bound onto Fe_3O_4@CNC hybrids was performed in the HEPES buffer (50 mM, pH 8.0) containing 0.3 M imidazole and 0.25 M NaCl. Finally, Fe_3O_4@CNC hybrids were remixed with copper ions for recycling. The purity of eluted lysozyme was confirmed via sodium

DOI: 10.1021/acs.biomac.6b01778
Biomacromolecules 2017, 18, 898−905

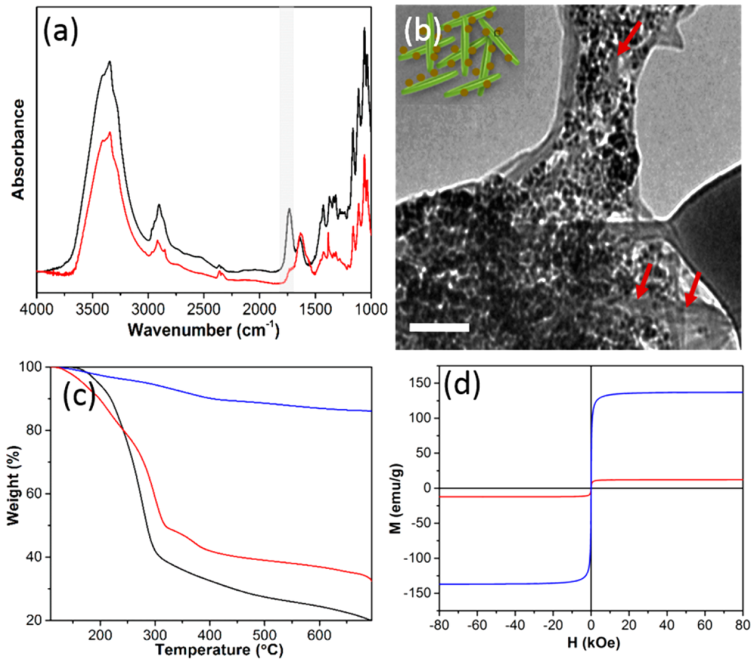

Figure 3. (a) FT-IR spectra of TEMPO-CNC and Fe_3O_4@CNC hybrids. The significant reduction of carboxyl peak contribution at 1730 cm^{-1} reveals that NH_2−Fe_3O_4 NPs cross-linked with TEMPO-CNC. (b) TEM image of Fe_3O_4@CNC hybrids to reveal the morphology after EDC/NHS coupling reaction (scale bar: 200 nm). Both NH_2- Fe_3O_4 NPs and TEMPO-CNC can be found. Red arrows indicate some of the rodlike TEMPO-CNC that are not covered by the NH_2−Fe_3O_4 NPs. Inset shows schematically the conjugation of NH_2−Fe_3O_4 NPs with TEMPO-CNC. (c) TGA curves of TEMPO-CNC, Fe_3O_4@CNC hybrids, and NH_2−Fe_3O_4 NPs showing the mass reduction as a function of temperature. (d) Hysteresis loops of Fe_3O_4@CNC hybrids and NH_2−Fe_3O_4 NPs at 300 K with diamagnetic contribution removed showing the magnetic response of Fe_3O_4@CNC hybrids. In panel a, c, and d, TEMPO-CNC, NH_2−Fe_3O_4 NPs, and Fe_3O_4@CNC hybrids are indicated in color as black, blue, and red profiles, respectively.

dodecyl sulfate polyacrylamide gel electrophoresis (SDS-PAGE, see Supporting Information).

RESULTS AND DISCUSSION

TEMPO-CNC. Typically, CNC produced by sulfuric acid hydrolysis contain about 1% sulfur (originated from the half-sulfate ester group on the surface).[40] These negatively charged groups have a positive impact on the stability of the resulting CNC aqueous dispersions (electrostatic repulsion). However, the presence of sulfate groups has a detrimental effect to the thermal stability of CNCs. Moreover, they can also contribute to the unwanted side reactions such as nucleophilic substitution and elimination. Therefore, we employed hydrochloric acid hydrolysis to produce sulfur-free CNC that were subsequently modified via TEMPO-mediated oxidation reaction to provide surface charges (COOH groups). The introduced carboxyl groups not only provide binding sites for the copper ions (in order to form the coordination complexes capable to selectively capture the protein lysozyme) but also serve as anchors for installing the magnetic NH_2−Fe_3O_4 nanoparticles via EDC/NHS-assisted coupling.[35,41] The morphology of TEMPO-CNC was characterized with AFM. The AFM image in Figure 2a reveals the rod-shaped TEMPO-CNC with approximate diameter of 5−10 nm and length of 100−200 nm. As expected, a new absorption band at 1730 cm^{-1} assigned to C═O stretching of carboxyl groups was observed and the TEMPO-CNC with degree of oxidation (DO) approximately 0.2 was confirmed using FT-IR. (Figure 3a, Supporting Information).

Amino-Functionalized Superparamagnetic Iron Oxide Nanoparticles (NH_2−Fe_3O_4 NPs). Several methods have been introduced for the preparation of magnetic iron oxide nanoparticles (Fe_3O_4 NPs).[42] Among them, the coprecipitation method is one of the most employed due to its scalability and feasibility.[43] In this work, superparamagnetic Fe_3O_4 NPs were synthesized via the chemical coprecipitation of iron salts (Fe^{3+} and Fe^{2+}). The dispensability and stability of the synthesized iron oxide nanoparticles are strongly dependent on their surface chemistry.[44] First, the OA−Fe_3O_4 NPs were synthesized via the chemical coprecipitation of iron salts (Fe^{3+} and Fe^{2+}). The hydrophobic OA−Fe_3O_4 NPs can be fully dispersed in nonpolar solvent such as toluene (Figure 2b). Subsequently, the NH_2−Fe_3O_4 NPs were prepared via ligand exchange. Dopamine presents a much stronger interaction with Fe atoms than oleic acid.[45] TEM image revealed spherical NH_2−Fe_3O_4 NPs with the mean size of 9.63 ± 1.73 nm (Figure 2c and Figure S2). It is worth noting that both OA−Fe_3O_4 NPs and NH_2−Fe_3O_4 NPs possess a good colloidal stability (over one month) in toluene and water (Figures S2 and S3) and an excellent magnetic response. The FT-IR spectra of dopamine-coated Fe_3O_4 NPs (NH_2−Fe_3O_4) and dopamine are presented in Figure 2d. The spectrum of dopamine exhibits a broad OH stretch in the range of 3300−3400 cm^{-1}. The bond of 3440 cm^{-1} in the NH_2−Fe_3O_4 NPs spectrum is attributed to an OH stretch due to surface absorbed water that through intermolecular bonding forms an iron hydroxide hydration shell.[46] The main vibration modes of dopamine such as the C−H vibration at 2925 cm^{-1}, C−O stretching of the phenolic OH at 1270 cm^{-1}, C═C ring stretching band at 1485 cm^{-1}, and the NH bending vibration of primary amine at 1620 cm^{-1} present in NH_2−Fe_3O_4 NPs spectrum as well.[47] In addition, the

DOI: 10.1021/acs.biomac.6b01778
Biomacromolecules 2017, 18, 898−905

electrokinetic potentials (zeta potential) of colloidal Fe_3O_4 NP dispersions were measured (see Supporting Information Figure S5). After undergoing a ligand exchange, the zeta potential shifted to +34.5 mV due to the installation of positively charged NH_3^+ groups.

Fe_3O_4@CNC hybrids. Collection and concentration of nanosized materials from the well-dispersed suspensions are often challenging. One way to overcome this issue is to activate the substrates with magnetic nanoparticles and collect them under the external magnetic field.[48] Our previous investigations have demonstrated the effective covalent conjugation of proteins, dyes, and nanoparticles with carboxylated nanofibrillated cellulose/cellulose nanocrystals through the well-established EDH/NHS-assisted coupling reaction.[49−51] In this work, we follow similar protocol to combine the amine-bearing magnetically responsive NH_2−Fe_3O_4 NPs and TEMPO-CNC to form the Fe_3O_4@CNC hybrids (Figure 1). FT-IR characterization exhibited a significant decrease (compared to that of TEMPO-CNC) in C═O stretching band at 1730 cm^{-1}; this is indicative of the amide formation between the amine groups of NH_2−Fe_3O_4 NPs and carboxyl groups of TEMPO-CNC (Figure 3a). The TEM image in Figure 3b displays both Fe_3O_4 NPs and TEMPO-CNC (indicated by red arrows). The magnetic properties of NH_2−Fe_3O_4 NPs and Fe_3O_4@CNC hybrids were measured using VSM technique at 300 K, as illustrated in Figure 3d, showing solid mass magnetization as a function of external field. The curves represent characteristic superparamagnetic behavior, that is, negligible magnetic hysteresis, high initial susceptibility and well-defined magnetic saturation in high external fields. The values of saturation magnetization (M_s) were 130 emu/g for NH_2−Fe_3O_4 NPs and 12.5 emu/g for Fe_3O_4@CNC hybrids, respectively. Obtained saturation magnetization values of NH_2−Fe_3O_4 NPs are comparable to those reported in the literature.[44] The content of Fe_3O_4 NPs was confirmed with thermogravimetric analysis (TGA) technique (Figure 3c). The weight loss (about 13%) of Fe_3O_4 NPs (blue curve) above 400 °C is due to the degradation of ligand molecules, that is, the loss of dopamine and coupled water. TEMPO-CNC presents rapid degradation above 280 °C, which is in agreement with the previously reported results.[35] The content of NH_2−Fe_3O_4 NPs in Fe_3O_4@CNC hybrids can be calculated to be ∼18% (Content % = $m_{\text{above 500 °C}}/m_{\text{initial}}$).

X-ray photoelectron spectroscopy (XPS) was employed to analyze the surface chemical composition of TEMPO-CNC, NH_2−Fe_3O_4 NPs, and Fe_3O_4@CNC hybrids. Wide range scans of TEMPO-CNC, NH_2−Fe_3O_4 NPs, and Fe_3O_4@CNC hybrids together with the high-resolution scans of Fe 2p and C 1s are shown in Figure 4. Cellulosic features, that is, oxygen and carbon peaks with the main carbon components at 286.7 and 288.1 eV in characteristic ratio, dominate the spectra of neat nanocrystal film and the hybrid material. The Fe 2p high-resolution image shows strong Fe 2p 3/2 and 2p1/2 bands at 711.0 and 724.6 eV binding energies for NH_2−Fe_3O_4 NPs. The high intensity values (18.8% Fe content, Table 1) suggests that the thin dopamine layer did not give rise to a loss of NH_2−Fe_3O_4 NPs magnetic properties. The nitrogen N 1s at 400 eV corresponds to −NH_2 groups of dopamine. These findings are in good agreement with the literature.[52] After the EDC/NHS coupling reaction, the bands of Fe 2p 3/2 and 2p1/2 at 711.0 and 724.6 eV binding energies decreased dramatically; this can be explained by the reduced amount of iron per gram of sample, that is, the amount of iron per total mass of the sample is less in Fe_3O_4@CNC hybrids. It should be mentioned that

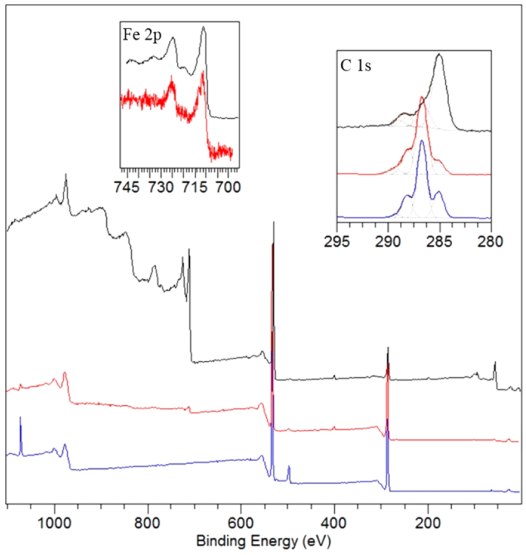

Figure 4. XPS wide spectra of NH_2−Fe_3O_4 NPs (black profile), Fe_3O_4−CNC hybrids (red profile), and TEMPO-CNC (blue profile). The insets represent the normalized high-resolution regions for C 1s and Fe 2p.

Table 1. Surface Elemental Compositions of Samples Presented in Figure 4

	atomic concentration (%)			
	C 1s	O 1s	Fe 2p	N 1s
TEMPO−CNC	60.9 ± 0.4	36.0 ± 0.8	0	0
NH_2−Fe_3O_4 NPs	35.0 ± 1.4	43.8 ± 1.2	18.8 ± 1.2	1.9 ± 0.1
Fe_3O_4@CNC hybrid	60.6 ± 0.5	37.1 ± 0.5	0.5 ± 0.1	1.5 ± 0.1

these findings in combination with those presented in Figure 3 strongly indicate the conjugation of NH_2−Fe_3O_4 NPs with TEMPO-CNC.

Complexation of Copper Ions with Fe_3O_4@CNC Hybrids. It is widely reported that cellulose can coordinate to metal ions such as Cr^{3+}, Cu^{2+}.[53] This unique property has been utilized for the separation of heavy metal ions. It is expected that the chelated copper ions are forming synergistic coordination complexes with carboxyl groups on TEMPO-CNC and amino groups from NH_2−Fe_3O_4 NPs, which in turn coordinately interact with imidazole rings from histidine residues exposed on protein surfaces.[54,55] This has been recently demonstrated by Zhu et al.[38] In this work, copper ions were complexed onto the Fe_3O_4@CNC hybrids at optimized pH 5[38] and the surface density of the immobilized copper ions was evaluated by UV−vis spectroscopy. The immobilized amount of copper ions was 41.1 ± 2 mg/g of hybrids as shown in Figure 5b (for comparison the maximum adsorption amount of copper ions is 110 mg/g of TEMPO-CNC), which is comparable with the reported literature.[38]

Lysozyme Separation from Aqueous Solution. Lysozyme can be obtained from animals, plants, and hen egg white and, as a unique enzyme, lysozyme possesses antimicrobial ability.[56] The role of the histidine residue in the active sites have been investigated.[57] In the present work, lysozyme was selected as a model protein because of its ability to selectively bind with copper. Zhu et al. reported that the adsorption capacity increased 4-fold after immobilizing copper ions on

DOI: 10.1021/acs.biomac.6b01778
Biomacromolecules 2017, 18, 898−905

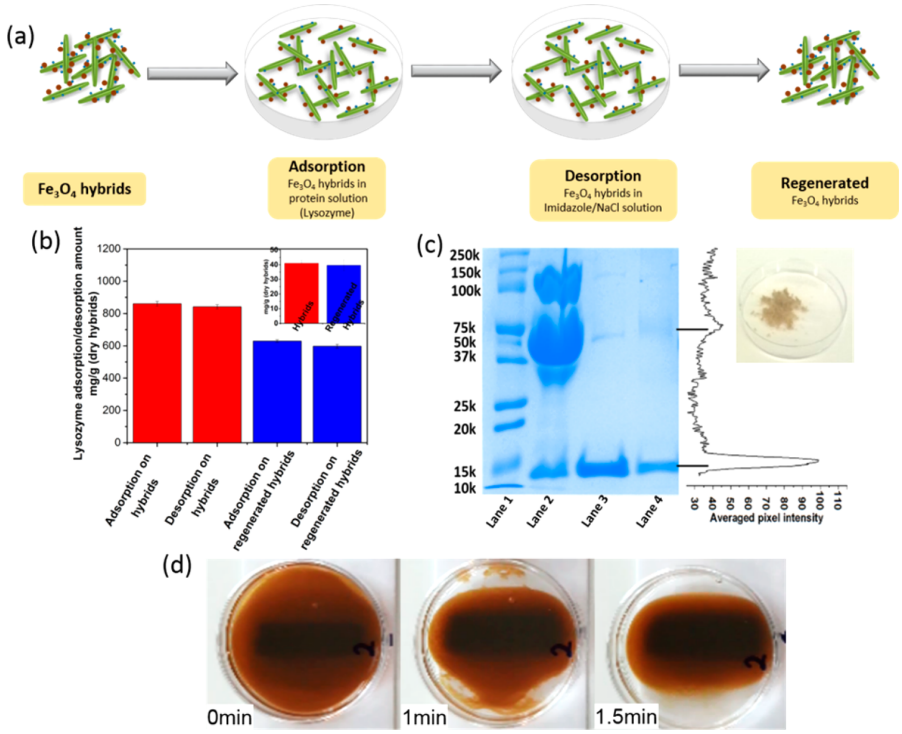

Figure 5. (a) Schematic illustration of adsorption/desorption process and regeneration of the Fe_3O_4@CNC hybrids. (b) Lysozyme adsorption and desorption. Red and blue color bars correspond to fresh and regenerated Fe_3O_4@CNC hybrids, respectively. Adsorption capacity of fresh hybrids (860.6 ± 14.8 mg/g) and regenerated Fe_3O_4@CNC hybrids (630.0 ± 8.7 mg/g). Desorption capacity of fresh hybrids (841.6 ± 13.5 mg/g) and regenerated Fe_3O_4@CNC hybrids (597.5 ± 12.8 mg/g). Inset: Immobilization capacity of copper ions. Fresh hybrids (41.05 ± 2 mg/g) and regenerated Fe_3O_4@CNC hybrids (39.6 ± 3.7 mg/g). (c) SDS-page analysis of molecular weight markers (Lane 1), egg white solution (Lane 2), commercial lysozyme after adsorption/desorption separation (Lane 3), and eluted lysozyme from egg white (Lane 4). The gel was stained with Coomassie Brilliant Blue (CBB). The intensity profiles of Lane 4 band shown in (c). Inset: photography of lyophilized lysozyme from egg white. (d) Snapshots showing the magnetic response of Fe_3O_4@CNC hybrids after mixing with lysozyme solution.

poly(vinyl alcohol-*co*-ethylene (PVA-*co*-PE) membrane.[38] The adsorption and desorption of lysozyme on the copper-complexed Fe_3O_4@CNC hybrids was performed in aqueous solution as illustrated in Figure 5a. The Fe_3O_4@CNC hybrids present an excellent lysozyme adsorption capacity reaching the maximum value of 860.6 ± 14.6 mg/$g_{(dry\ Fe3O4@CNC\ hybrids)}$ (Figure 5b). For purposes of comparison, the lysozyme adsorption capacity of copper-free Fe_3O_4@CNC hybrids was found to be about 393 mg/g (owing to the electrostatic interactions between the negatively charged chelating groups and the positively charged lysozyme molecules). Therefore, the high lysozyme adsorption capacity on the copper-complexed Fe_3O_4@CNC hybrids is attributed to the specific affinity between the immobilized copper ions and lysozyme molecules. It should also be noted that the observed lysozyme adsorption capacity is 3-fold higher than those reported in the literature.[38] This notable improvement in the lysozyme adsorption could be due to the large surface area of CNC, which in turn provides an increased amount of binding sites for lysozyme capture. Moreover, it should be mentioned that the Fe_3O_4@CNC hybrids experienced a rapid response to the external magnetic field (Figure 5d and Supporting Video).

Efficient elution and facile regenerability are essential features for sustainable separation techniques. To evaluate the elution efficiency, the lysozyme containing Fe_3O_4@CNC hybrids were dispersed in elution media containing 0.3 M NaCl and 0.25 M imidazole for 2 h. It was found that up to 841.6 ± 13.5 mg/$g_{(dry\ hybrids)}$ of adsorbed lysozyme can be eluted, which corresponds to 97.8% elution efficiency (Figure 5b). Moreover, the recyclability was investigated by regenerating the used Fe_3O_4@CNC hybrids via extensive washing and recomplexation with 25 mM copper ions. The adsorption capacity of the regenerated Fe_3O_4@CNC hybrids is found to be 630 ± 8.7 mg/$g_{(dry\ hybrids)}$ and up to 95% of the adsorbed lysozyme could still be eluted (Figure 5b). Finally, the purity of separated lysozyme was determined with SDS-PAGE analysis, which revealed a narrow band approximately at 14.3 kDa (Figure 5c, Lane 3). The adsorption capacity may be further improved by altering the lysozyme concentration, the pH of the medium, adsorption temperature, and/or the ionic strength of the lysozyme solution.[38]

Lysozyme Separation from the Egg White. To evaluate the performance of copper-complexed Fe_3O_4@CNC hybrids in practical environments, lysozyme separation was carried out in the presence of chicken egg white. As shown in Figure 5c (lane 2), the major protein components in chicken egg white are ovotransferrin, ovalbumin, ovomucoid, and lysozyme with molecular weights of 78, 45, 28, and 14 kDa, respectively.[38,58] After performing the lysozyme separation by using the synthesized Fe_3O_4@CNC hybrids (see details in Experimental Section and Supporting Information), the SDS PAGE analysis revealed only one strong protein band at 14.3 kDa. (Figure 5c, Lane 4). This indicates that the lysozyme was selectively isolated from the complex mixture of proteins. Moreover, the

DOI: 10.1021/acs.biomac.6b01778
Biomacromolecules 2017, 18, 898−905

purity of isolated lysozyme was found to be higher than 90%, as determined from the intensity profiles of the band (Lane 4) by measuring the height and the width of the signals and subtracting the noise from the background signals (Figure 5c). Finally, the isolated lysozyme protein was lyophilized. (Figure 5c)

CONCLUSIONS

We present an efficient approach to synthesize magnetically responsive Fe_3O_4@CNC hybrids with immobilized metal, which displays a significant affinity for selective protein separation. Magnetic Fe_3O_4@CNC hybrids were prepared by EDC/NHS-assisted coupling of TEMPO-CNC and NH_2−Fe_3O_4 NPs. The Fe_3O_4@CNC hybrids complexed with copper ions provided specific binding sites for proteins, for example, lysozyme. The performance of magnetic Fe_3O_4@CNC hybrids was assessed by separating lysozyme from an aqueous matrix. The lysozyme binding capacity of Fe_3O_4@CNC hybrids was found to be 860.6 ± 14.6 mg/g and 97.8% of the adsorbed protein was recovered by elution. The regenerated Fe_3O_4@CNC hybrids were efficiently reutilized for protein isolation. The remarkable results obtained in this work demonstrate the potential of Fe_3O_4@CNC hybrids carrying copper ions for selective protein separation from complex systems.

ASSOCIATED CONTENT

Supporting Information

The Supporting Information is available free of charge on the ACS Publications website at DOI: 10.1021/acs.biomac.6b01778.

Video of lysozyme separation with the assistance of magnet (AVI)

Experimental procedures of protein concentration analysis, SDS page analysis. TEM image of TEMPO-oxidation cellulose nanocrystals (TEMPO-CNC). Calculation method of degree of oxidation of TEMPO-CNC. The calibration curve for copper ions concentration. Zeta potential of NH_2−Fe_3O_4 NPs. Stability test of Fe_3O_4 NPs (PDF)

AUTHOR INFORMATION

Corresponding Author

*E-mail: erkko.filpponen@aalto.fi.

ORCID

Jiaqi Guo: 0000-0001-7557-0356

Ilari Filpponen: 0000-0003-0538-6523

Orlando J. Rojas: 0000-0003-4036-4020

Notes

The authors declare no competing financial interest.

ACKNOWLEDGMENTS

This work was supported by the Academy of Finland through its Centres of Excellence Programme (2014−2019). The authors thank Dr. Taneli Tiittanen (Department of Chemistry, Aalto University) for the help with TGA measurement. Dr. Joseph Campbell is acknowledged for performing the XPS analysis. Mrs. Anu Anttila is thanked for the experimental assistance.

REFERENCES

(1) Li, B.; Jiang, B.; Boyce, B. M.; Lindsey, B. A. Multilayer Polypeptide Nanoscale Coatings Incorporating IL-12 for the Prevention of Biomedical Device-Associated Infections. *Biomaterials* **2009**, *30*, 2552−2558.

(2) Li, Y.; Lin, T.; Luo, Y.; Liu, Q.; Xiao, W.; Guo, W.; Lac, D.; Zhang, H.; Feng, C.; Wachsmann-Hogiu, S. A Smart and Versatile Theranostic Nanomedicine Platform Based on Nanoporphyrin. *Nat. Commun.* **2014**, *5*, 4712.

(3) Steinbakk, M.; Naess-Andresen, C.; Fagerhol, M.; Lingaas, E.; Dale, I.; Brandtzaeg, P. Antimicrobial Actions of Calcium Binding Leucocyte L1 Protein, Calprotectin. *Lancet* **1990**, *336*, 763−765.

(4) Zarling, J. M.; Moran, P. A.; Haffar, O.; Sias, J.; Richman, D. D.; Spina, C. A.; Myers, D. E.; Kuebelbeck, V.; Ledbetter, J. A.; Uckun, F. M. Inhibition of HIV Replication by Pokeweed Antiviral Protein Targeted to CD4 Cells by Monoclonal Antibodies. *Nature* **1990**, *347*, 92−95.

(5) Cormack, B. P.; Valdivia, R. H.; Falkow, S. FACS-Optimized Mutants of the Green Fluorescent Protein (GFP). *Gene* **1996**, *173*, 33−38.

(6) Maruyama, K.; Natori, R.; Nonomura, Y. New Elastic Protein from Muscle. *Nature* **1976**, *262*, 58−60.

(7) Hoshino, T.; Nakamura, H.; Okamoto, M.; Kato, S.; Araya, S.; Nomiyama, K.; Oizumi, K.; Young, H. A.; Aizawa, H.; Yodoi, J. Redox-Active Protein Thioredoxin Prevents Proinflammatory Cytokine-or Bleomycin-Induced Lung Injury. *Am. J. Respir. Crit. Care Med.* **2003**, *168*, 1075−1083.

(8) Habibi, Y.; Lucia, L. A.; Rojas, O. J. Cellulose Nanocrystals: Chemistry, Self-Assembly, and Applications. *Chem. Rev.* **2010**, *110*, 3479−3500.

(9) Brinkmann, A.; Chen, M.; Couillard, M.; Jakubek, J. Z.; Leng, T.; Johnston, J. L. Correlating Cellulose Nanocrystal Particle Size and Surface Area. *Langmuir* **2016**, *32* (24), 6105−6114.

(10) Heath, L.; Thielemans, W. Cellulose Nanowhisker Aerogels. *Green Chem.* **2010**, *12*, 1448−1453.

(11) Annamalai, P. K.; Dagnon, K. L.; Monemian, S.; Foster, E. J.; Rowan, S. J.; Weder, C. Water-Responsive Mechanically Adaptive Nanocomposites Based on Styrene−Butadiene Rubber and Cellulose Nanocrystals-Processing Matters. *ACS Appl. Mater. Interfaces* **2014**, *6*, 967−976.

(12) Podsiadlo, P.; Choi, S.; Shim, B.; Lee, J.; Cuddihy, M.; Kotov, N. A. Molecularly Engineered Nanocomposites: Layer-by-Layer Assembly of Cellulose Nanocrystals. *Biomacromolecules* **2005**, *6*, 2914−2918.

(13) Lagerwall, J. P.; Schütz, C.; Salajkova, M.; Noh, J.; Park, J. H.; Scalia, G.; Bergström, L. Cellulose Nanocrystal-Based Materials: from Lliquid Crystal Self-Assembly and Glass Formation to Multifunctional Thin Films. *NPG Asia Mater.* **2014**, *6*, e80.

(14) Shopsowitz, K. E.; Hamad, W. Y.; MacLachlan, M. J. Chiral Nematic Mesoporous Carbon Derived from Nanocrystalline Cellulose. *Angew. Chem., Int. Ed.* **2011**, *50*, 10991−10995.

(15) Li, M.; Wu, Q.; Song, K.; Qing, Y.; Wu, Y. Cellulose Nanoparticles as Modifiers for Rheology and Fluid Loss in Bentonite Water-Based Fluids. *ACS Appl. Mater. Interfaces* **2015**, *7*, 5006−5016.

(16) Way, A. E.; Hsu, L.; Shanmuganathan, K.; Weder, C.; Rowan, S. J. pH-Responsive Cellulose Nanocrystal Gels and Nanocomposites. *ACS Macro Lett.* **2012**, *1*, 1001−1006.

(17) Xiong, R.; Lu, C.; Wang, Y.; Zhou, Z.; Zhang, X. Nanofibrillated Cellulose as the Support and Reductant for the Facile Synthesis of Fe_3O_4/Ag Nanocomposites with Catalytic and Antibacterial Activity. *J. Mater. Chem. A* **2013**, *1*, 14910−14918.

(18) Li, Y.; Zhu, H.; Gu, H.; Dai, H.; Fang, Z.; Weadock, N. J.; Guo, Z.; Hu, L. Strong Transparent Magnetic Nanopaper Prepared by Immobilization of Fe_3O_4 Nanoparticles in a Nanofibrillated Cellulose Network. *J. Mater. Chem. A* **2013**, *1*, 15278−15283.

(19) Nypelö, T.; Rodriguez-Abreu, C.; Rivas, J.; Dickey, M. D.; Rojas, O. J. Magneto-Responsive Hybrid Materials Based on Cellulose Nanocrystals. *Cellulose* **2014**, *21*, 2557−2566.

(20) Olsson, R. T.; Samir, M. A.; Salazar-Alvarez, G.; Belova, L.; Ström, V.; Berglund, L. A.; Ikkala, O.; Nogues, J.; Gedde, U. W.

DOI: 10.1021/acs.biomac.6b01778
Biomacromolecules 2017, 18, 898−905

Making Flexible Magnetic Aerogels and Stiff Magnetic Nanopaper Using Cellulose Nanofibrils as Templates. *Nat. Nanotechnol.* **2010**, *5*, 584−588.
(21) Lu, A.; Salabas, E. e.; Schüth, F. Magnetic Nanoparticles: Synthesis, Protection, Functionalization, and Application. *Angew. Chem., Int. Ed.* **2007**, *46*, 1222−1244.
(22) Abu-Reziq, R.; Alper, H.; Wang, D.; Post, M. L. Metal Supported on Dendronized Magnetic Nanoparticles: Highly Selective Hydroformylation Catalysts. *J. Am. Chem. Soc.* **2006**, *128*, 5279−5282.
(23) Gao, J.; Gu, H.; Xu, B. Multifunctional Magnetic Nanoparticles: Design, Synthesis, and Biomedical Applications. *Acc. Chem. Res.* **2009**, *42*, 1097−1107.
(24) Arruebo, M.; Fernández-Pacheco, R.; Ibarra, M. R.; Santamaría, J. Magnetic Nanoparticles for Drug Delivery. *Nano Today* **2007**, *2*, 22−32.
(25) Jun, Y.; Lee, J.; Cheon, J. Chemical Design of Nanoparticle Probes for High-Performance Magnetic Resonance Imaging. *Angew. Chem., Int. Ed.* **2008**, *47*, 5122−5135.
(26) Hergt, R.; Dutz, S.; Müller, R.; Zeisberger, M. Magnetic Particle Hyperthermia: Nanoparticle Magnetism and Materials Development for Cancer Therapy. *J. Phys.: Condens. Matter* **2006**, *18*, S2919.
(27) Wang, Y.; Wang, G.; Xiao, Y.; Yang, Y.; Tang, R. Yolk−Shell Nanostructured Fe_3O_4@ $NiSiO_3$ for Selective Affinity and Magnetic Separation of His-Tagged Proteins. *ACS Appl. Mater. Interfaces* **2014**, *6*, 19092−19099.
(28) Xu, F.; Geiger, J. H.; Baker, G. L.; Bruening, M. L. Polymer Brush-Modified Magnetic Nanoparticles for His-tagged Protein Purification. *Langmuir* **2011**, *27*, 3106−3112.
(29) Xu, C.; Xu, K.; Gu, H.; Zhong, X.; Guo, Z.; Zheng, R.; Zhang, X.; Xu, B. Nitrilotriacetic Acid-Modified Magnetic Nanoparticles as a General Agent to Bind Histidine-Tagged Proteins. *J. Am. Chem. Soc.* **2004**, *126*, 3392−3393.
(30) Lee, I. S.; Lee, N.; Park, J.; Kim, B. H.; Yi, Y.; Kim, T.; Kim, T. K.; Lee, I. H.; Paik, S. R.; Hyeon, T. Ni/NiO Core/Shell Nanoparticles for Selective Binding and Magnetic Separation of Histidine-Tagged Proteins. *J. Am. Chem. Soc.* **2006**, *128*, 10658−10659.
(31) Marchessault, R. H.; Bremner, G; Chauve, G. Fishing for Proteins with Magnetic Cellulosic Nanocrystals. In *Polysaccharides for Drug Delivery and Pharmaceutical Applications*; Marchessault, R. H., Ravenelle, F, Zhu, X., Eds.; American Chemical Society: Washington, DC, 2006; Volume *934*, pp 3−17.
(32) Anirudhan, T. S.; Rejeena, S. R. Selective Adsorption of Hemoglobin Using Polymer-Grafted-Magnetite Nanocellulose Composite. *Carbohydr. Polym.* **2013**, *93*, 518−527.
(33) Mahmoud, K. A.; Lam, E.; Hrapovic, S.; Luong, J. H. Preparation of Well-Dispersed Gold/Magnetite Nanoparticles Embedded on Cellulose Nanocrystals for Efficient Immobilization of Papain Enzyme. *ACS Appl. Mater. Interfaces* **2013**, *5*, 4978−4985.
(34) Araki, J.; Wada, M.; Kuga, S.; Okano, T. Flow Properties of Microcrystalline Cellulose Suspension Prepared by Acid Treatment of Native Cellulose. *Colloids Surf., A* **1998**, *142*, 75−82.
(35) Saito, T.; Isogai, A. TEMPO-Mediated Oxidation of Native Cellulose. The Effect of Oxidation Conditions on Chemical and Crystal Structures of the Water-Insoluble Fractions. *Biomacromolecules* **2004**, *5*, 1983−1989.
(36) Filpponen, I.; Argyropoulos, D. S. Regular Linking of Cellulose Nanocrystals via Click Chemistry: Synthesis and Formation of Cellulose Nanoplatelet Gels. *Biomacromolecules* **2010**, *11*, 1060−1066.
(37) Yao, G.; Liang, R.; Huang, C.; Wang, Y.; Qiu, J. Surface Plasmon Resonance Sensor Based on Magnetic Molecularly Imprinted Polymers Amplification for Pesticide Recognition. *Anal. Chem.* **2013**, *85*, 11944−11951.
(38) Zhu, J.; Sun, G. Facile Fabrication of Hydrophilic Nanofibrous Membranes with an Immobilized Metal−Chelate Affinity Complex for Selective Protein Separation. *ACS Appl. Mater. Interfaces* **2014**, *6*, 925−932.
(39) Kent, M.; Yim, H.; Sasaki, D.; Satija, S.; Seo, Y.; Majewski, J. Adsorption of Myoglobin to Cu (II)-IDA and Ni (II)-IDA Functionalized Langmuir Monolayers: Study of the Protein Layer Structure during the Adsorption Process by Neutron and X-ray Reflectivity. *Langmuir* **2005**, *21*, 6815−6824.
(40) Beck-Candanedo, S.; Roman, M.; Gray, D. G. Effect of Reaction Conditions on the Properties and Behavior of Wood Cellulose Nanocrystal Suspensions. *Biomacromolecules* **2005**, *6*, 1048−1054.
(41) Orelma, H.; Johansson, L.; Filpponen, I.; Rojas, O. J.; Laine, J. Generic Method for Attaching Biomolecules via Avidin−Biotin Complexes Immobilized on Films of Regenerated and Nanofibrillar Cellulose. *Biomacromolecules* **2012**, *13*, 2802−2810.
(42) Gupta, A. K.; Gupta, M. Synthesis and Surface Engineering of Iron Oxide Nanoparticles for Biomedical Applications. *Biomaterials* **2005**, *26*, 3995−4021.
(43) Laurent, S.; Forge, D.; Port, M.; Roch, A.; Robic, C.; Vander Elst, L.; Muller, R. N. Magnetic Iron Oxide Nanoparticles: Synthesis, Stabilization, Vectorization, Physicochemical Characterizations, and Biological Applications. *Chem. Rev.* **2008**, *108*, 2064−2110.
(44) Qu, H.; Caruntu, D.; Liu, H.; O'Connor, C. J. Water-Dispersible Iron Oxide Magnetic Nanoparticles with Versatile Surface Functionalities. *Langmuir* **2011**, *27*, 2271−2278.
(45) Xu, C.; Xu, K.; Gu, H.; Zheng, R.; Liu, H.; Zhang, X.; Guo, Z.; Xu, B. Dopamine as a Robust Anchor to Immobilize Functional Molecules on the Iron Oxide Shell of Magnetic Nanoparticles. *J. Am. Chem. Soc.* **2004**, *126*, 9938−9939.
(46) Shultz, M. D.; Reveles, J. U.; Khanna, S. N.; Carpenter, E. E. Reactive Nature of Dopamine as a Surface Functionalization Agent in Iron Oxide Nanoparticles. *J. Am. Chem. Soc.* **2007**, *129*, 2482−2487.
(47) Mazur, M.; Barras, A.; Kuncser, V.; Galatanu, A.; Zaitzev, V.; Turcheniuk, K. V.; Woisel, P.; Lyskawa, J.; Laure, W.; Siriwardena, A. Iron Oxide Magnetic Nanoparticles with Versatile Surface Functions Based on Dopamine Anchors. *Nanoscale* **2013**, *5*, 2692−2702.
(48) Chen, W.; Chen, Y. Functional Fe_3O_4@ZnO Magnetic Nanoparticle-Assisted Enrichment and Enzymatic Digestion of Phosphoproteins from Saliva. *Anal. Bioanal. Chem.* **2010**, *398*, 2049−2057.
(49) Orelma, H.; Morales, L. O.; Johansson, L.; Hoeger, I. C.; Filpponen, I.; Castro, C.; Rojas, O. J.; Laine, J. Affibody Conjugation onto Bacterial Cellulose Tubes and Bioseparation of Human Serum Albumin. *RSC Adv.* **2014**, *4*, 51440−51450.
(50) Orelma, H.; Johansson, L.; Filpponen, I.; Rojas, O. J.; Laine, J. Generic Method for Attaching Biomolecules via Avidin−Biotin Complexes Immobilized on Films of Regenerated and Nanofibrillar Cellulose. *Biomacromolecules* **2012**, *13*, 2802−2810.
(51) Junka, K.; Guo, J.; Filpponen, I.; Laine, J.; Rojas, O. J. Modification of Cellulose Nanofibrils with Luminescent Carbon Dots. *Biomacromolecules* **2014**, *15*, 876−881.
(52) Yuan, Y.; Rende, D.; Altan, C. L.; Bucak, S.; Ozisik, R.; Borca-Tasciuc, D. Effect of Surface Modification on Magnetization of Iron Oxide Nanoparticle Colloids. *Langmuir* **2012**, *28*, 13051−13059.
(53) Huang, C.; Chen, J.; Tsai, T.; Hsieh, Y.; Lin, K. A. Dual-Functionalized Cellulose Nanofibrils Prepared Through TEMPO-Mediated Oxidation and Surface-Initiated ATRP. *Polymer* **2015**, *72*, 395−405.
(54) Browne, W. J.; North, A.; Phillips, D.; Brew, K.; Vanaman, T. C.; Hill, R. L. A Possible Three-Dimensional Structure of Bovine α-Lactalbumin Based on that of Hen's Egg-White Lysozyme. *J. Mol. Biol.* **1969**, *42*, 65−86.
(55) Wu, C.; Suen, S.; Chen, S.; Tzeng, J. Analysis of Protein Adsorption on Regenerated Cellulose-Based Immobilized Copper Ion Affinity Membranes. *J. Chromatogr. A* **2003**, *996*, 53−70.
(56) Chang, H.; Yang, C.; Chang, Y. Rapid Separation of Lysozyme from Chicken Egg White by Reductants and Thermal Treatment. *J. Agric. Food Chem.* **2000**, *48*, 161−164.
(57) Kravchenko, N.; Kleopina, G.; Kaverzneva, E. Investigation of the Active Sites of Lysozyme. Carboxymethylation of the Imidazole Group of Histidine and of the ϵ-Aminogroup of Lysine. *Biochim. Biophys. Acta, Spec. Sect. Enzymol. Subj.* **1964**, *92*, 412−414.
(58) Desert, C.; Guerin-Dubiard, C.; Nau, F.; Jan, G.; Val, F.; Mallard, J. Comparison of Different Electrophoretic Separations of Hen Egg White Proteins. *J. Agric. Food Chem.* **2001**, *49*, 4553−4561.

DOI: 10.1021/acs.biomac.6b01778
Biomacromolecules 2017, 18, 898−905